Carbon nanotube reinforced supramolecular gels with electrically conducting, viscoelastic and near-infrared sensitive properties†

Suman K. Samanta,[a] Asish Pal,[a] Santanu Bhattacharya*[a] and C. N. R. Rao*[b]

Received 23rd February 2010, Accepted 30th April 2010
DOI: 10.1039/c0jm00491j

Pristine and long-chain functionalized single-walled carbon nanotubes (SWNTs) were incorporated successfully in supramolecular organogels formed by an all-*trans* tri(*p*-phenylenevinylene) bis-aldoxime to give rise to new nanocomposites with interesting mechanical, thermal and electrical properties. Variable-temperature UV-vis and fluorescence spectra reveal both pristine and functionalized SWNTs promote aggregation of the gelator molecules and result in quenching of the UV-vis and fluorescence intensity. Electron microscopy and confocal microscopy show the existence of a densely packed and directionally aligned fibrous network in the resulting nanocomposites. Differential scanning calorimetry (DSC) of the composites shows that incorporation of SWNTs increases the gel formation temperature. The DSC of the xerogels of **1**–SWNT composites indicates formation of different thermotropic mesophases which is also evident from polarized optical microscopy. The reinforced aggregation of the gelators on SWNT doping was reflected in the mechanical properties of the composites. Rheology of the composites demonstrates the formation of a rigid and viscoelastic solid-like assembly on SWNT incorporation. The composites from gel–SWNTs were found to be semiconducting in nature and showed enhanced electrical conductivity compared to that of the native organogel. Upon irradiation with a near IR laser at 1064 nm for 5 min it was possible to selectively induce a gel-to-sol phase transition of the nanocomposites, while irradiation for even 30 min of the native organogel under identical conditions did not cause any gel-to-sol conversion.

Introduction

Among the nanomaterials, carbon nanotubes (CNTs) and related systems have attracted a lot of attention due to their high aspect ratio, extraordinary mechanical properties and enhanced electrical conductivity which make them useful in many aspects ranging from optoelectronics to even in biomedical applications.[1] Accordingly CNT based research is being increasingly driven towards developing superior conducting materials as CNTs are good electrical conductors themselves.[2] CNT doping has been also exploited for improving flame-retardant performances, achieving enhanced conductivity,[3] electrostatic charging,[4] optical emitting devices,[5] and in lightweight, high strength composites[6] *etc*.

Although the CNTs are difficult to solubilize in various solvent media, they can interact with different classes of compounds by forming supramolecular complexes which in turn render them dispersible in that medium.[7] Polymers, especially those with aromatic moieties, interact with the CNTs since they can impart a π–π stacking interaction with the nanotube walls, thereby, solubilizing the nanotubes in the medium.[8] Proteins,[9] DNA[10] and other biomolecules have been also shown to solubilize SWNTs in aqueous solution.

In this context the low molecular mass organogelators (LMOGs)[11] constitute an interesting class of soft materials such as physical gels, which are thermoreversible and are swollen in a liquid in which they are gelated. Their structure is "cross-linked" by supramolecular interactions (coulombic, hydrogen bond, van der Waals *etc.*). These materials have fibrillar networks which contain microporous pockets filled with solvent molecules which can host various nanomaterials such as nanoparticles, nanotubes *etc*. Fukushima *et al.* reported that when SWNTs were mixed with imidazolium ion-based room-temperature ionic liquids, the resulting materials transformed into gels.[12] Currently there is a strong interest in the investigations where CNTs have been incorporated in hydrogel, organogel and polymeric matrices.[13]

We have previously reported that the incorporation of metal nanoparticles modulates the properties of the gel–Au/Ag nanoparticle composites depending on the 'information inscribed' on the nanoparticle surface as capping agent.[14] Recently, we described a novel gel–nanotube composite system from a

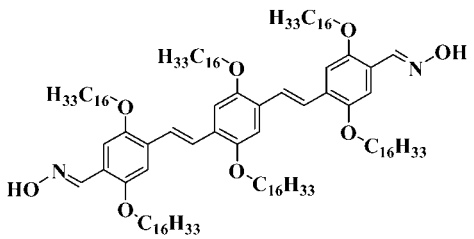

Chart 1 Molecular structure of the gelator **1** used in the present study.

[a]*Department of Organic Chemistry, Indian Institute of Science, Bangalore, India. E-mail: sb@orgchem.iisc.ernet.in; Fax: +91-80-23600529; Tel: +91-80-22932664*
[b]*Chemistry and Physics of Materials Unit, Jawaharlal Nehru Centre for Advanced Scientific Research, Bangalore, India. E-mail: cnrrao@jncasr.ac.in*

† Electronic supplementary information (ESI) available: Characterization of the CNTs. See DOI: 10.1039/c0jm00491j

non-chromophoric organogelator based on a fatty acid amide of L-alanine and SWNTs.[15] However, the L-alanine based gelator was devoid of any aromatic moiety and as a consequence possessed only a limited ability to disperse CNTs. In order to improve the efficient incorporation of CNTs in gels, herein we employ a luminescent organogel containing a conjugated *p*-phenylenevinylene based aromatic chromophore, **1** (Chart 1),[16] which acts as an excellent host for both pristine SWNTs (Pr-SWNTs) and *n*-hexadecyl amide functionalized SWNTs (C_{16}-SWNTs). We examined the influence of CNT incorporation on the aggregation properties of **1**, which demonstrated nanotube encapsulated self-assembled structures indicating the formation of fiber-reinforced supramolecular networks of gel–SWNT nanocomposites. Importantly the resulting gel–SWNT composites showed increased electrical conducting properties, improved viscoelasticity and a remarkable NIR induced thermoreversible gel-to-sol transition behaviour.

Experimental

Materials

All reagents, starting materials and silica gel for TLC and column chromatography were obtained from the best known commercial sources and were used without further purification, as appropriate. Solvents were distilled and dried prior to use. Pristine single-walled carbon nanotubes (SWNTs) were synthesized by the arc discharge method from graphite and purified by treatment with concentrated HCl (to remove iron catalyst) and further hydrogen treatment at 900 °C in a furnace oven as described.[17] The functionalized SWNTs have been synthesized as reported earlier[15] and the characterization data of the SWNTs are presented in the electronic supporting information (ESI†). The gelator **1** has been synthesized as reported earlier.[16]

Gelation studies

A solution of gelator (**1**) in toluene, which also contained dispersed SWNTs, was heated in a water-bath at 60 °C in a test-tube to make a clear sol. The sol was sonicated for 5 min at 60 °C, and upon cooling under ambient conditions for 20 min formed a gel stable to inversion of the test-tube.

Confocal microscopy

A diluted toluene solution of **1** (1×10^{-4} M) incorporated with 1.64 wt% SWNTs was drop casted on a pre-cleaned glass slide and it was left overnight for drying in a dust-free environment and finally evacuated to remove all the solvent. In another glass slide the same toluene solution of **1** incorporated with SWNTs (50 μL) was put and kept for 15 min at low temperature (0 °C). The confocal images were taken on a Leica TCS SP5 (Germany) microscope with an excitation wavelength of 488 nm.

Scanning and transmission electron microscopy

The physical gel of **1** and the gel–SWNT composites were carefully scooped onto the brass stubs and were allowed to dry under ambient condition. In another experiment the gel samples of **1** and SWNTs composites were scooped onto the brass stubs and were allowed to freeze-dry. The samples were then coated with gold vapor and analyzed on a Quanta 200 SEM operated at 10 kV. Diluted toluene solution of each sample was drop-casted onto a carbon coated copper grid (200 mesh size) and the TEM images were taken at an accelerating voltage of 300 kV using TECNAI F30 and JEOL JEM 3010 instruments.

UV-vis and fluorescence spectroscopy

UV-vis and fluorescence spectra of the solution of **1** in the presence and absence of CNTs were recorded on Shimadzu model 2100 spectrophotometer and Hitachi F-4500 spectrofluorimeter, respectively.

Differential scanning calorimetry of gel and gel–CNT composites

Organogel and the soft gel–SWNT composite samples were prepared as mentioned above and their thermotropic properties was investigated using high sensitivity differential scanning calorimetry using a CSC-4100 model multi-cell Differential Scanning Calorimeter (Calorimetric Sciences Corporation, Utah, USA).

Gels and the gel–SWNT composites were heated to the sol state and 0.4 mL clear sols were taken into DSC ampoules. The ampoules were cooled, sealed and the gels were allowed to set under ambient conditions. The calorimetric measurements were carried out in the temperature range of 10–60 °C at a scan rate of 20 °C h^{-1}. At least two to three consecutive heating and cooling scans were performed to ensure reproducibility. Baseline thermograms were obtained using the same amount of solvent in the DSC cells. The thermograms for the gel were obtained by subtracting the respective baseline thermogram from the sample thermogram using 'CpCalc' software provided by the manufacturer.

Differential scanning calorimetry of dried composites

Xerogel–SWNT composites were prepared by evaporating the solvents under high vacuum in ambient condition from the gel–SWNT composite sample (5 mg of **1** incorporated with 0.1 mg SWNTs in 0.5 mL toluene). The transition temperatures were determined using a Differential Scanning Calorimeter (DSC; Perkin-Elmer, Model Pyris 1D) with heating and cooling rate fixed at 5 °C min^{-1} for all the measurements. This technique was used to detect the thermal transitions and to monitor the rate of heat flow from the sample during phase changes in the temperature range of 25–150 °C.

Polarized optical microscopy (POM)

The morphology of the nanocomposites during the thermal transitions was observed using POM as follows. 0.2 mL of gel alone (10 mg mL^{-1} of **1**) or its SWNT-nanocomposite (0.1 mg of SWNTs dispersed in a solution of 5 mg of **1** in 0.5 ml toluene) were placed on a glass slide and the respective samples were allowed to dry under ambient conditions. Then each sample was covered using a cover-slip and the changes in their optical textures were observed using polarized light microscopy (Olympus BX51) equipped with a heating stage (Mettler

FP82HT) and a central processor (Mettler FP90). The heating and cooling rate was fixed at 1 °C min^{-1} for all the samples.

Rheological studies

An Anton Paar 100 rheometer using a cone and plate geometry (CP 25-2) was utilized. The gap distance between the cone and the plate was fixed at 0.05 mm. The gel was scooped on the plate of the rheometer. Stress amplitude sweep experiments were performed at a constant oscillation frequency of 1 Hz for the strain range 0.001–100 at 20 °C. Oscillatory frequency sweep experiments were performed with each sample in the linear viscoelastic region to ensure that the calculated parameters correspond to an intact network structure. The rheometer has a built-in computer which converts the torque measurements into G' (the storage modulus) and G'' (the loss modulus) in oscillatory shear experiments.

Current (*I*)–voltage (*V*) measurements

Various gel–SWNT composites containing different concentrations of SWNTs were prepared separately by the dispersion of 0.1 or 0.5 mg of SWNTs in 10 mg mL^{-1} of **1** in toluene. The blank SWNTs samples were prepared by the dispersion of 0.1 mg of either SWNT sample (Pr-SWNTs or C_{16}-SWNTs) in 1 mL of toluene. 20 μL of each sample was drop-casted on separate gold sputtered glass plates having an electrode gap of 30 μm, and allowed to dry in a dust-free environment for overnight. Finally the samples were further dried *in vacuo* and the *I*–*V* characteristics of each sample were measured using a DC source electrometer (Keithley sourcemeter model 2400).

NIR laser irradiation

A sample of 0.4 mL of the organogel and different gel–SWNT composite samples were taken on separate quartz cuvette of path length 1 cm. The samples were irradiated for different lengths of time using a 1064 nm laser (600 mW) in a CW Nd:YAG 1064 nm laser source under ambient conditions.

Results and discussion

In the present study we have employed a gelator (**1**) based on tri-*p*-phenylenevinylene (TPV) skeleton where two termini are functionalized with oxime residues. Such end groups provide hydrogen-bonding donor and acceptor sites allowing favorable interactions leading to supramolecular self-assembly. **1** forms a stable organogel in toluene and 'weak' gels in *n*-dodecane. The aggregation and resulting gelation of **1** is induced by van der Waals interactions among long hydrocarbon chains, π–π stacking among conjugated aromatic moieties, and weak hydrogen bonding interactions among peripheral hydroxyl groups.[16,18]

TPV derivatives have excellent properties to form aligned layers since the backbone of TPV contains three benzene rings and should therefore be a natural choice for the solubilization of CNTs. CNT have a π aromatic surface which could further stabilize the assembly of the gelator molecules through π–π stacking interactions. This prompted us to incorporate pristine

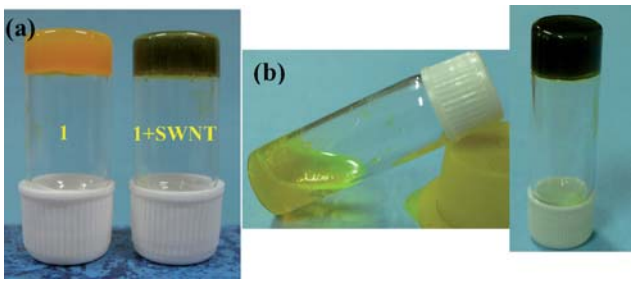

Fig. 1 (a) Photograph of a toluene gel of **1** and its composite with Pr-SWNT. (b) Photograph of the viscous solution of **1** in toluene below its MGC (left) and with Pr-SWNT incorporation it turns in to a gel (right).

SWNTs and hexadecyl chain functionalized SWNTs in the gel matrix. The toluene gel of **1** alone is yellow in color and upon incorporation of SWNTs turns greenish black (Fig. 1a). The toluene solution of **1** taken in a test tube, just below its minimum gelator concentration (MGC) appeared to be viscous but not a gel as perhaps expected. Interestingly the incorporation of a small amount of pristine SWNT (1.5 wt%) converted the mixture into a rigid gel such that the mass did not flow under gravity (Fig. 1b). This signifies that there must be a definite role of SWNTs in rigidifying the assembly *via* their intimate interactions with the gelator molecules. The gel of **1** in toluene, above its MGC, could be used as a scaffold to incorporate increasing quantities of SWNTs (~6 wt%) beyond which the SWNT started to phase separate.

Morphology of the gel–SWNT composites

Microscopic studies. Various microscopic studies were undertaken to observe the morphology of the SWNT reinforced gel-nanocomposites. The luminescent nature of the gelator molecules allowed us to observe the superstructures created in the gel-nanocomposites under a confocal microscope. When excited at 488 nm, the xerogel fibers showed red emission and the presence of three-dimensional fiber bundles (diameter ~5–6 μm) was clearly observed (Fig. 2a–c). Notably, for the

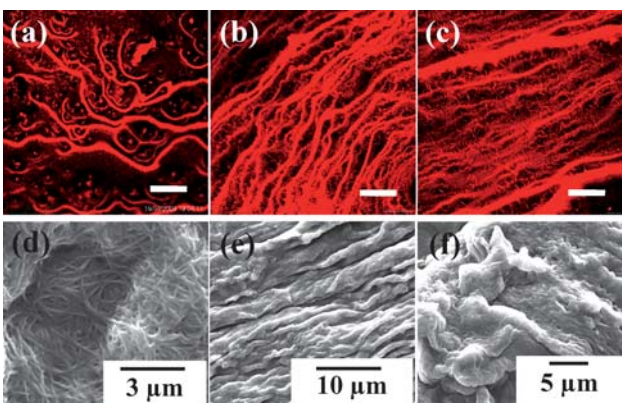

Fig. 2 Confocal microscopic images (excitation at 488 nm) of dried fibers of (a) **1**, (b) **1**–Pr-SWNT and (c) **1**–C_{16}-SWNT composites from toluene at 25 °C; [**1**] = 1×10^{-4} M and 1.64 wt% SWNTs added (scale bar 10 μm). SEM images of dried toluene gel of (d) **1**, (e) **1** + 0.25 wt% of Pr-SWNT and (f) **1** + 0.25 wt% C_{16}-SWNT.

nanocomposites with the incorporation of 1.64 wt% of either Pr-SWNT or C_{16}-SWNT, the fibers showed more ordered structures. Interestingly, the fibers of the composites showed a clear alignment in a certain direction compared to the native gel fiber where there was no such directionality. We have also performed confocal microscopy with actual gels prepared in toluene (without drying). In the wet condition the fiber formation from gels (with the solvent) was confirmed, as well as the directionality of the fiber formation, which was retained as seen under a confocal microscope. Also, the fiber diameters increased in case of the nanocomposites upon incorporation of CNTs (Fig. S2d–f, ESI†).

Scanning electron microscopy (SEM) of a dried toluene gel of **1** revealed a three-dimensional fibrous network with fiber diameter of ~200–300 nm, but with the incorporation of Pr-SWNT the resulting nanocomposite showed collation of the individual fibers into bundles (Fig. 2d–f). Also, the bundles of fibers appeared to align themselves in a directional fashion. Even with the incorporation of C_{16}-SWNT (having hexadecyl chains attached to the CNT scaffold) into the organogel network made the resulting fibrous network denser and thicker due to collation of thin fibers into bundles, which are similar with other types of gel–SWNT composite reported earlier.[15,19] In order to compare our results, we further performed the SEM experiment with the gel and the nanocomposites under freeze-dried conditions. With the freeze-dried samples, the observed morphologies are in accordance with the results obtained using the air-dried gel samples. The directionality and the collation of fibers were also observed in case of the nanocomposites (Fig. S2a–c, ESI†).

This suggests that in presence of SWNTs, the gelator molecules interact strongly with the exposed π-surface of the SWNTs leading them to form bundles of fibers in a directional fashion. Further evidence of interaction between **1** and SWNTs was observed using transmission electron microscopy (TEM). TEM images of **1** in toluene show fibrillar networks with fiber diameters in the range 20–100 nm and the toluene dispersed Pr-SWNTs show bundles of nanotubes (Fig. 3). Upon incorporation of SWNTs, the fibers of the gel network further bundled to produce thicker fibers. The wrapping of nanotubes by the gelator molecules was observed for both **1**–Pr-SWNT and **1**–C_{16}-SWNT nanocomposites (shown by arrows). Thus the nanocomposites show fiber encapsulated nanotubes with increased fiber diameter which appear as the SWNT reinforced gel network.

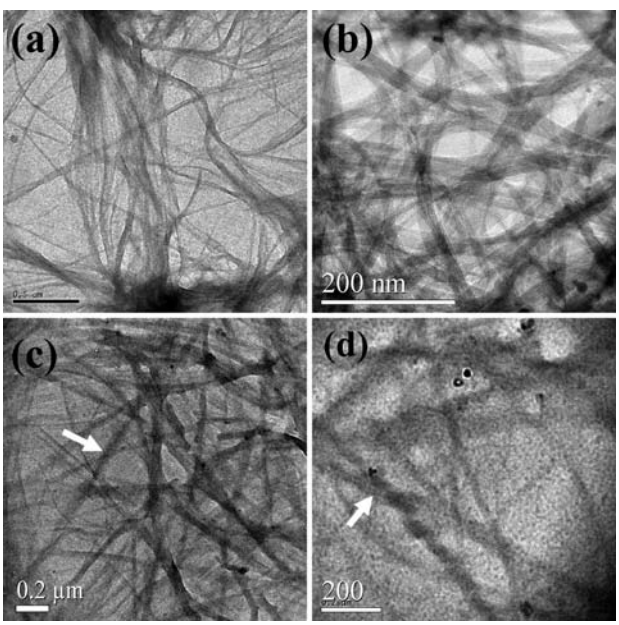

Fig. 3 TEM images of (a) **1**, (b) Pr-SWNT, (c) **1**–Pr-SWNT and (d) **1**–C_{16}-SWNT.

Interaction of SWNTs with TPV gelator molecules in solution

UV-vis and fluorescence studies. To understand the aggregation process that induces the formation of the gel and gel-nanocomposites, UV-vis spectra of **1** and mixtures of **1** with SWNTs were investigated in the solution phase. *n*-Dodecane was chosen as the solvent as even at very low concentrations of **1**, the propensity to its aggregation was quite high. The absorption maximum (λ_{max}) of **1** in *n*-dodecane (1×10^{-5} M) was observed at 440 nm at 15 °C in addition to a shoulder band at 490 nm. Upon increase in temperature, the intensity of the absorption band at 440 nm increased progressively with the gradual loss of the shoulder band (Fig. 4a). In the temperature range of 30–35 °C, the shoulder band at 490 nm was completely lost with the production of a blue-shifted band at 430 nm indicating an apparent 'breakdown' of the aggregates of **1** in *n*-dodecane.[16] Upon incorporation of 0.1 mg mL^{-1} of either Pr-SWNT or C_{16}-SWNT in the solution of **1**, the intensity of the absorption maxima diminished at lower temperature showing a broad maxima at 450 nm with a shoulder band at 500 nm for either version of SWNTs.[13c] Interestingly, with increasing temperature (even up to 65 °C) the corresponding spectra did not show any significant increase in the absorption intensity although a gradual blue-shift occurs with the shoulder band starting to diminish above 50 °C (Fig. 4b and c). This indicates formation of aggregated species by strong interaction of SWNTs with **1** through π–π interactions *via* aromatic moieties and additionally through van der Waals interactions with the *n*-hexadecyl side chains of gelators and C_{16}-SWNTs.

The fluorescence spectra of **1** in *n*-dodecane (1×10^{-5} M) showed a less intense emission between 450–560 nm at the lower temperature region of 15–30 °C (Fig. 4d). Upon gradual increase in temperature, two clear emission maxima at 480 and 515 nm appeared with a substantial increase in the emission intensity.[16] Addition of either type of SWNTs to the solution of **1** resulted in a decrease of the corresponding emission intensity. The observed fluorescence quenching is presumably a consequence of SWNT induced aggregation of **1** because CNTs are known to be strong fluorescence quenchers.[20] On heating the mixture, up to 40 °C there was a slight increase in the broad emission and beyond that, two peaks at 480 and 515 nm were clearly observable (Fig. 4e and f). Further increase in the temperature made the emission intensity higher, though notably, the fluorescence intensities of the composites were found to be always lower than that of gelator **1** alone. Thus on incorporation of SWNTs, the gelator molecules no longer remain as individual species and rather

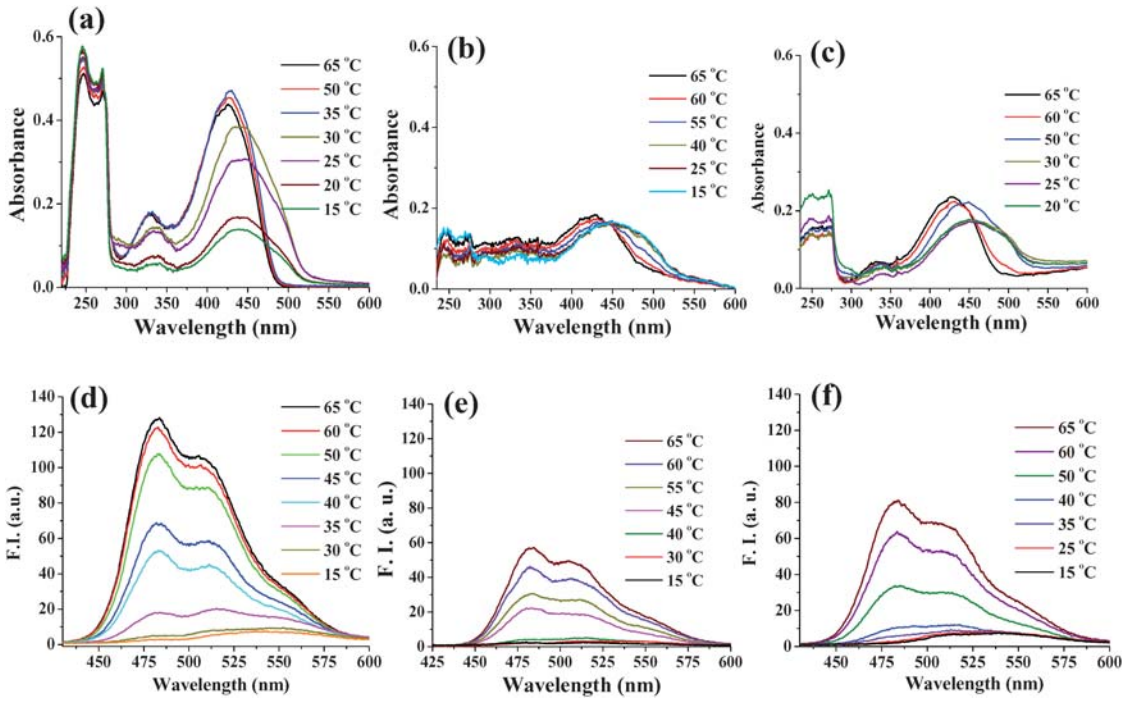

Fig. 4 Variable-temperature UV-vis and fluorescence spectra of (a, d) **1**, (b, e) **1**–Pr-SWNT and (c, f) **1**–C_{16}-SWNT in *n*-dodecane, respectively; [**1**] = 1 × 10^{-5} M and 0.1 mg mL^{-1} SWNTs added (for emission spectra λ_{ex} = 420 nm).

become a part of the supramolecular assembly encompassing the SWNTs.

Differential scanning calorimetry (DSC)

Organogel and its SWNT composites. The thermotropic behavior of the gel-nanocomposites has been investigated in order to figure out the influence of SWNTs on the nanocomposites. Possibly due to its limited dispersibility and propensity to precipitate during heating and cooling, no significant changes in the thermal properties were observed in the nanocomposites made of pristine SWNTs.[15] Whereas, in the case of nanocomposites made of C_{16}-SWNT, an increase in the gel formation temperature (T_f) was observed in the DSC cooling scans, although the heating scans did not show any significant changes. Also the sol-to-gel transition temperature (T_f) increased with the increase in the amount of C_{16}-SWNT incorporated in the gel matrix. The organogel alone showed a T_f at 24.4 °C, while the composite with 1.96 wt% of C_{16}-SWNT showed T_f at 27.0 °C (Fig. 5a). On increasing the amount of C_{16}-SWNT (3.84 wt%) in the composite the T_f increased further to 27.5 °C.

The sol-to-gel formation process for the gel alone is brought about by cooling the sol of **1** to ~24 °C. In the case of composite gels, the sol-to-gel conversion occurs at higher temperature (>27 °C). Thus the presence of carbon nanotubes facilitates the formation of gel from the sol at a temperature the gel alone exists as a sol. This implies that nanotubes aid nucleation of the gelator molecules and therefore help inter-gelator self-assembly even at a higher temperature.[21] Thus it is possible that C_{16}-SWNT with hexadecyl chains matched with the gelator molecules structurally and served as the nuclei so as to decrease the nucleation energy barrier of the gelator, thereby increasing the sol-to-gel formation temperatures for the nanocomposites. This, in turn, explains the facilitation in gel forming ability in presence of SWNTs even at concentrations lower than the MGC of the gelator **1**.

DSC of xerogel and its SWNT composites. Since aggregates derived from TPV based molecules are known to show the presence of different thermotropic mesophases,[22] the dried gels and the composites were further investigated under DSC. When cooling from the molten state the xerogel of **1** showed a phase-transition at 129.1 °C followed by another phase transition at 114.4 °C (Fig. 5b). The presence of more than one phase in the dried gel sample may be inferred from the observation of three peaks at 92.6, 126.5 and 135.8 °C in the heating cycle. In the case of dry composites of **1**–Pr-SWNT two peaks at 79.1 and 125.6 °C were seen in the heating cycle and one major broad peak at 113.5 °C was observed in the cooling cycle. The dry **1**–C_{16}-SWNT composite showed the presence of two prominent peaks at 90.6 and 126.5 °C followed by a broad peak at 133.7 °C in the heating cycle and only one peak at 115.4 °C in the cooling cycle. The incorporation of the SWNTs caused a shift toward a lower transition temperature both in the heating and cooling cycle for the dry composite samples indicating a change in the organization of the composites from the native gel.[23] Thus the doping of the SWNTs in xerogels of **1** can modify the supramolecular aggregation of the composites, which brings about the appearance of different phases as the macroscopic changes.

Polarized optical microscopy (POM). The DSC results prompted us to examine thermotropic mesophases in the composites under a polarized optical microscope. Under polarized light the dried gel of **1** showed the presence of birefringent textures upon cooling from the isotropic melt (Fig. 6). This

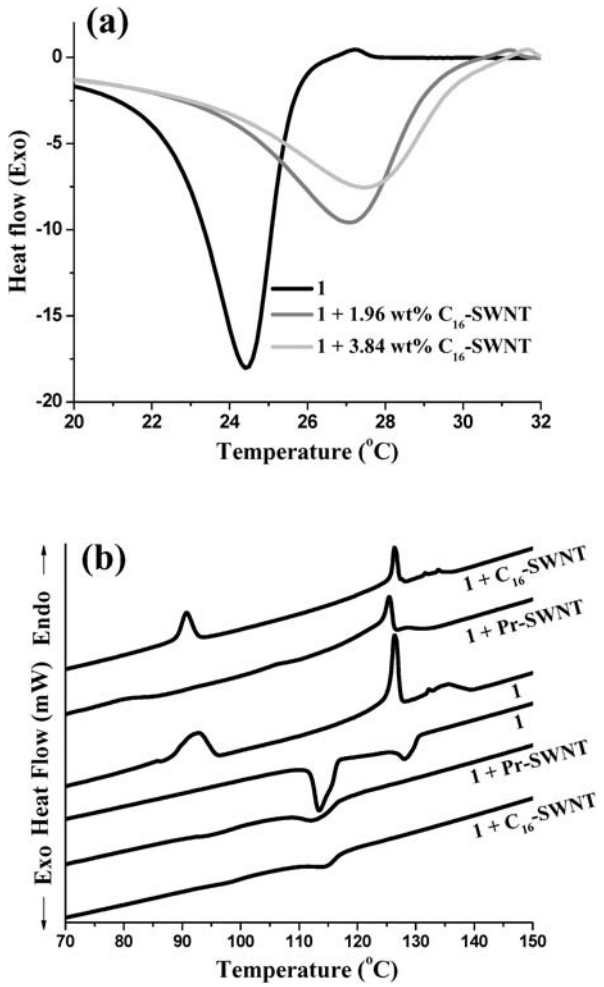

Fig. 5 DSC curves for (a) the exothermic scan of compound **1** and C_{16}-SWNT composite in toluene and (b) the xerogel of compound **1** and composites with Pr-SWNT and C_{16}-SWNT (1.96 wt% SWNTs added).

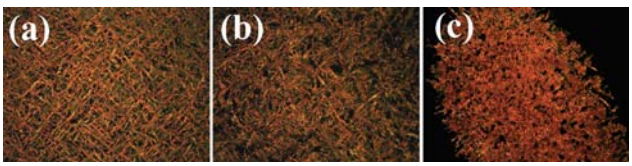

Fig. 6 Different types of birefringent phases for (a) **1**, (b) **1**–Pr-SWNT and (c) **1**–C_{16}-SWNT when cooling from the isotropic phase (1.96 wt% SWNTs added, temperature 125 °C, magnification ×20).

indicated an anisotropic growth of the three-dimensional aggregates by the TPV molecules leading to the formation of different mesophases. Interestingly, the gel-nanocomposites of **1**–Pr-SWNT showed the existence of fewer birefringent textures in the specimen with the change in the textures compared to that of **1**.[24] Whereas, the birefringence was retained in the case of xerogel composite of **1**-C_{16}-SWNT compared to **1** although a significant change in its texture was observed. Probably due to the presence of flexible hexadecyl chains in C_{16}-SWNT, which can interact with the long chains of **1**, the anisotropic growth of the gelator was influenced by the C_{16}-SWNT in the composite.

The anisotropic growth of the gelator molecules in the presence and absence of SWNTs were further monitored by taking snapshots at progressively decreasing temperatures from the isotropic melt which showed different birefringent textures for the nanocomposites compared to that of the xerogel (Fig. S3–S5, ESI†). Also, a clear change in the birefringent texture with temperature corresponding to the peak observed in the DSC cooling scan was observed for the xerogel and the nanocomposites. Under cooling condition the samples were scratched with an external assistance which showed that the samples were rotating above 115 °C confirming the liquid-crystalline nature, while below that temperature the samples were not rotated, indicating a crystalline state has reached.

Rheological studies

To examine the influence of SWNT incorporation in the gel of **1** and to find out the change in the viscoelastic parameters, rheological studies were undertaken. The flow behavior of the viscoelastic materials were measured by oscillatory frequency sweep experiment, where the storage and the loss moduli G' and G'', respectively, were measured as a function of angular frequency at a fixed strain of 0.01%.[25] Fig. 7a shows the variation

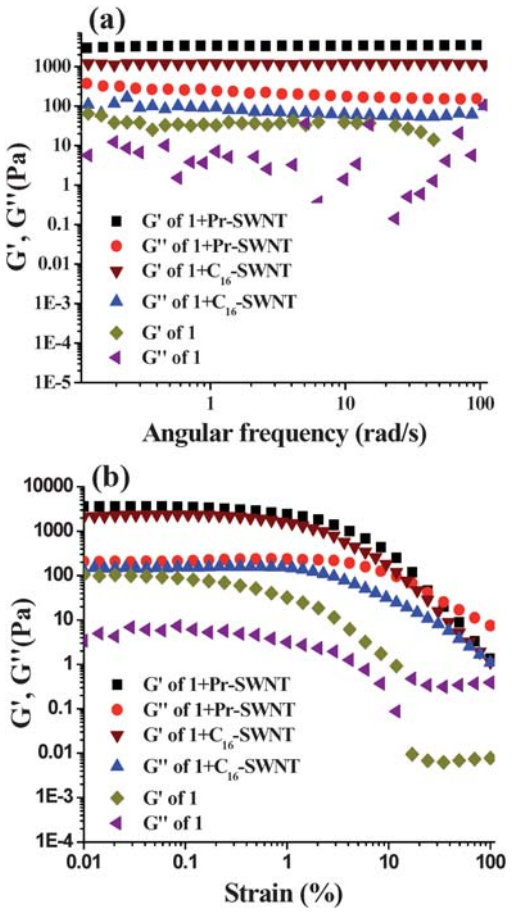

Fig. 7 Comparative oscillatory frequency sweep experiments (a) and oscillatory amplitude sweep experiments (b) of toluene gel of **1** (5 mg mL^{-1}) alone and in gel–SWNT composites containing 0.25 wt% of SWNT.

of G' and G'' with angular frequency for the gel–nanotube composite as compared to native toluene gel of **1**. The native gel at its minimum gelator concentration showed the characteristics of a relatively 'weak' gel with G' greater than G''. The signals due to storage and loss moduli were found to be noisy due to the weak gel character at the MGC of the gel of **1**. Interestingly, upon incorporation of 0.25% of either the Pr-SWNT or the C_{16}-SWNT, both the moduli showed >20 times increase in magnitude and exhibited a pronounced plateau over the entire angular frequency range. This suggests formation of a more viscoelastic solid-like material upon doping of the SWNT in gel even at the MGC of the gelator.[26]

Strain amplitude sweeps shown in Fig. 7b also revealed the elastic response of the gel and the gel–SWNT nanocomposites. The elastic moduli (G') for both the samples with gel at its MGC gradually decreased with increasing strain and above the critical strain region there was a crossover of G' and G'' indicating a disruption and collapse of the gel state. In line with the frequency sweep experiment, here also, both the elastic and loss moduli of the nanocomposites showed significantly higher magnitude than that of the native gel of **1** in toluene. Also, the critical strain region, where the crossover takes place, is much greater in the nanocomposites ($\gamma \sim 30\%$) than that in organogel alone ($\gamma \sim 9\%$). This clearly indicates greater resistance to flow behavior upon addition of either form of SWNT into the gel. Also, when the SWNTs were incorporated in different proportions in the toluene gel network of **1** with the gelator concentration greater than the MGC, the oscillatory frequency sweep measurement showed a monotonous rise in the elastic moduli of the resulting nanocomposite with increasing percentage of the pristine SWNT doping (Fig. 8a) which is in line with the reports obtained from other gel–nanotube composites.[13a,15] The amplitude sweep experiment for the composites containing various percentages of the Pr-SWNT also showed a monotonous rise in the elastic modulus and the yield stress value with the greater loading of SWNTs (Fig. 9a). This signifies that up to a certain percentage of SWNT loading (beyond which excess SWNTs start to phase separate from the gel matrix) the nanocomposite gradually was rendered more rigid and condensed in terms of the mechanical strength. Similarly, when the C_{16}-SWNT was doped in the toluene gel of **1** in varying weight percentages, the frequency sweep experiment on the resulting nanocomposites showed a gradual and monotonous increase in the plateau value of G' with increasing percentage of C_{16}-SWNT (Fig. 8b). The oscillatory amplitude sweep experiments on the nanocomposites revealed a monotonous increase in the G' and yield stress values with increasing percentage of the C_{16}-SWNT (Fig. 9b).

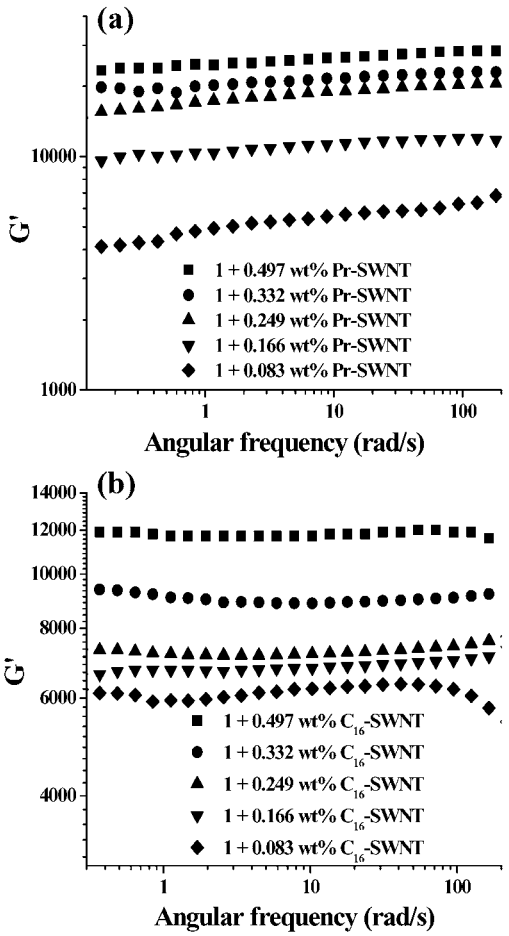

Fig. 8 Comparison of G' of **1**-SWNT composites ([**1**] = 10 mg mL^{-1}) with varying wt% of (a) pristine SWNT and (b) C_{16}-SWNT in toluene from oscillatory frequency sweep experiment.

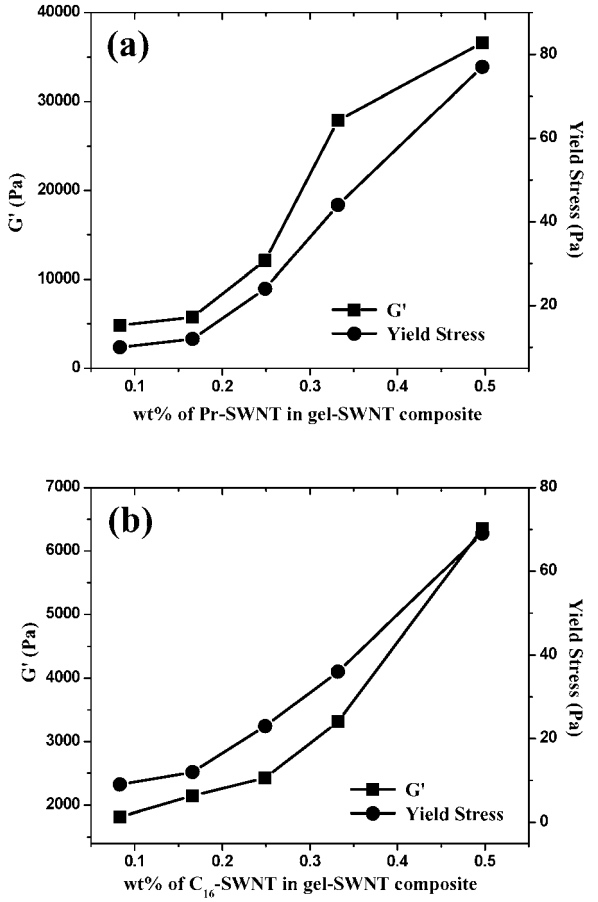

Fig. 9 Plot of G' and yield stress of **1**–SWNT composites with varying weight percentage of (a) Pr-SWNT and (b) C_{16}-SWNT in the respective composites; [**1**] in toluene = 10 mg mL^{-1}.

Electrical conductivity (current (*I*)–voltage (*V*)) measurements

Since the gelator **1** has extensive π-electron conjugation in its backbone, such a molecule should be ideal to impart stacking interactions with the CNTs through its aromatic surface. Accordingly, we thought that it would be interesting to investigate the electrical conductivity behaviour of the gel–SWNTs composites. Accordingly, the *I*–*V* measurements for the dried gel of **1**, **1**–SWNT composites as well as individual SWNTs have been measured. In the low voltage region (~1–2 V) the curve followed Ohm's law ($V/I = R$) (the linear region of the curve) and the corresponding resistance (R) was calculated from the *I*–*V* curve by using the law.[27] For all the samples in the higher voltage region, the *I*–*V* characteristic did not show a linear relationship indicating a deviation from Ohm's law behavior. This type of *I*–*V* characteristic is typical of semiconducting materials and the *I*–*V* curves obtained here indicate the semiconducting nature of the SWNTs[28] as well as that of the dried gel of **1** and the gel–SWNTs composites. The current (I) and the corresponding calculated resistance (R) at a voltage (V) of 10 V are recorded in Table 1.

The amount of current generated upon application of the voltage on the two-probe electrode has been recorded for the xerogel of **1** and composites with Pr-SWNT and C_{16}-SWNT. The current observed for xerogel of **1** was 7.6×10^{-9} A whereas in the case of the **1**–Pr-SWNT composite it was 2.1×10^{-8} A and for **1**–C_{16}SWNT the value was 1.3×10^{-8} A (Fig. 10a). When the Pr-SWNT concentration was further increased, I increased appreciably to a value of 5.5×10^{-5} A indicating significant increments in the flow of current. Comparatively higher orders of magnitude of current were obtained in the case of only Pr-SWNT or C_{16}-SWNT (5.6×10^{-3} and 7.4×10^{-7} A, respectively) (Fig. 10b). Thus, the magnitude of current has increased in the case of composites with either version of SWNTs. This suggests participation of SWNTs in the conducting process in the nanocomposites through π–π stacking interactions. However, it should be noted that, the experimental values of current were several orders of magnitude greater in the case of Pr-SWNT or C_{16}-SWNT samples than that of the xerogel of **1** or the composites. Furthermore, the magnitude of current is several orders higher for Pr-SWNT than that of the *n*-hexadecyl amide functionalized SWNT, presumably due to the loss of integrity of SWNTs upon covalent functionalization.[29] So the increment in the current, or in turn decrease in the resistance, for the **1**-SWNT composites is probably owing to the formation of a more ordered aggregated fiber in the xerogel of the composites which is evident from the microscopy images.

Table 1 Summary of current and resistance at a voltage of 10 V for different samples obtained from *I*–*V* curve

	Current/A	Resistance/Ω
1	7.6×10^{-9}	2×10^{9}
1 + 0.99 wt% Pr-SWNT	2.1×10^{-8}	7×10^{8}
1 + 0.99 wt% C_{16}-SWNT	1.3×10^{-8}	1×10^{9}
1 + 4.76 wt% Pr-SWNT	5.5×10^{-5}	2.5×10^{5}
Pr-SWNT	5.6×10^{-3}	4×10^{3}
C_{16}-SWNT	7.4×10^{-7}	2×10^{7}

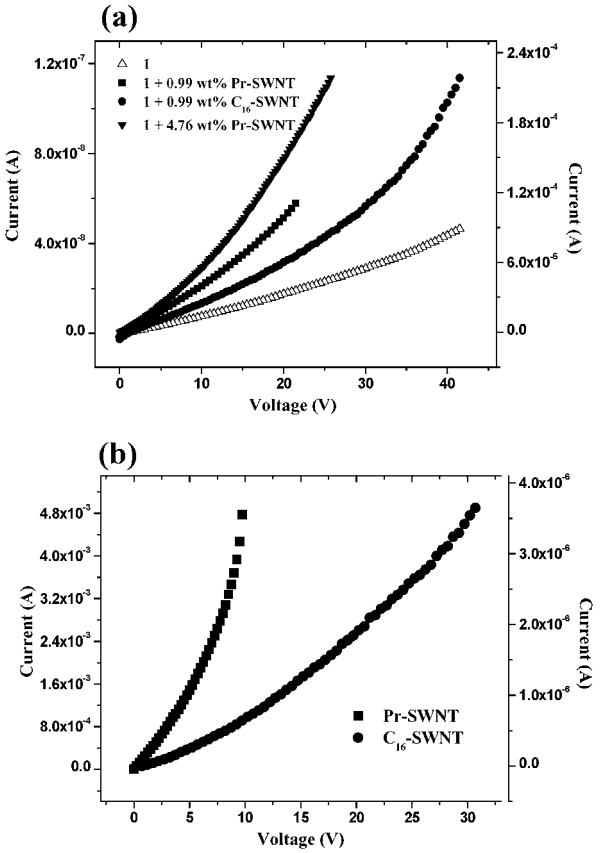

Fig. 10 *I*–*V* measurements of (a) **1**, **1** + 0.99 wt% Pr-SWNT and **1** + 0.99 wt% C_{16}-SWNT (left *y*-axis) and **1** + 4.76 wt% Pr-SWNT (right *y*-axis) and (b) current of Pr-SWNT alone (left *y*-axis) and C_{16}-SWNT alone (right *y*-axis).

NIR laser irradiation studies

The nanocomposites were further subjected to near-IR radiation to explore how such an external stimuli[30] interacts with the sample. NIR radiation which is transparent and unreactive to biological systems (unlike UV-vis) could be used as stimuli for controlled release applications, drug delivery,[31] NIR responsive light modulated materials and in selective control of microfluidics.[32] Since SWNTs are known to absorb in the NIR region and can show NIR laser driven exothermicity,[10b] it could be exploited in developing smart gel–CNT composites. Both the gel and the nanocomposites were accordingly irradiated with a focused laser beam (Nd:YAG, $\lambda = 1064$ nm) at 25 °C. The gel–SWNT composites upon NIR laser irradiation exhibited a gel-to-sol phase transition whereas the native TPV based gel did not collapse even after 30 min of exposure to NIR irradiation under identical condition (Fig. 11). This took ~5 min for the **1**–Pr-SWNT (0.5 wt%) gel sample whereas for the **1**–C_{16}-SWNT (0.5 wt%) composite the gel-to-sol transition was complete within 2 min of NIR irradiation. The SWNTs having characteristic van Hove peaks in the NIR region (700–1100 nm) are known to absorb NIR light and get heated up due to their high thermal conductivity.[15] The melted gel–CNT materials on standing at 25 °C for 10 min reverted back to the gel state with partial separation of the dispersed Pr-SWNT from the gel. However, on

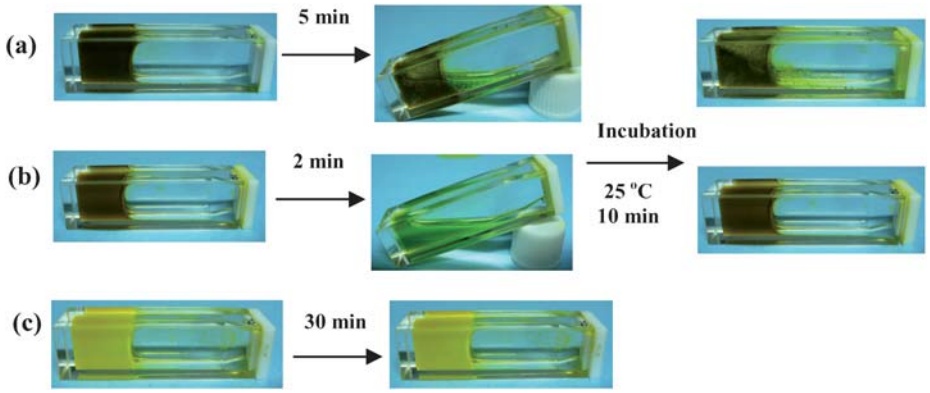

Fig. 11 Effect of NIR laser triggered on (a) **1**–Pr-SWNT, (b) **1**–C_{16}-SWNT and (c) native gel at 25 °C.

sonication post-NIR irradiation Pr-SWNTs can be fully redispersed in the same gel sample. In contrast, no phase separation was seen in the gel reformed from C_{16}-SWNT doped gels. Since C_{16}-SWNTs are more homogeneously dispersed in the gel NIR driven heating of the matrix was more efficient than for the composite containing Pr-SWNTs.

Conclusions

In this paper, we describe the synthesis of SWNT/organogel composites and evaluation of their properties. The properties of nanotube/organogel composites depend on a multitude of factors that include the type (pristine or functionalized SWNT) of nanotube loading, dispersion state and alignment of nanotubes in the gel matrix, and the interfacial interactions between the SWNTs and the TPV gelator molecules. The TPV-based chromophore provides an additional handle to probe SWNT-induced aggregation of gelator molecules and thermochromism using UV-vis and fluorescence spectroscopy. Functionalization of nanotubes provides a convenient route to improve dispersion and modify interfacial properties that in turn improves the NIR sensitivity properties of nanocomposites. However, composites made of pristine CNT have superior mechanical and electrical conducting properties compared to its long-chain functionalized analogues. CNTs have clearly demonstrated their capability as conductive fillers in gel nanocomposites. Further advances with respect to electrical conductivity in nanotube/gel composites are likely only if metallic nanotubes could be used in the nanocomposites.

In summary, nanotube/organogel composites offer both significant potential and challenges, marking it as a vibrant area of work for years to come. The improvement and application of these composites will depend on how effectively we can handle these challenges.

Acknowledgements

This work was supported by J. C. Bose fellowship award of DST to S. B. S. K. S thanks CSIR for a senior research fellowship. We thank Department of Physics, INI, RRI and JNCASR for various Instrumental facilities and Prof. V. Natarajan for giving access to the NIR laser facility.

Notes and references

1 (*a*) C. N. R. Rao and A. Govindaraj, *Nanotubes and Nanowires*, RSC Publishing, Cambridge, UK, 2005; (*b*) Z. Liu, W. Cai, L. He, N. Nakayama, K. Chen, X. Sun, X. Chen and H. Dai, *Nat. Nanotechnol.*, 2007, **2**, 47; (*c*) Z. Zhang, X. Yang, Y. Zhang, B. Zeng, S. Wang, T. Zhu, R. B. Roden, Y. Chen and R. Yang, *Clin. Cancer Res.*, 2006, **12**, 4933; (*d*) R. Singh, D. Pantarotto, D. McCarthy, O. Chaloin, J. Hoebeke, C. D. Partidos, J.-P. Briand, M. Prato, A. Bianco and K. Kostarelos, *J. Am. Chem. Soc.*, 2005, **127**, 4388; (*e*) A. Bianco, K. Kostarelos, C. D. Partidos and M. Prato, *Chem. Commun.*, 2005, 571; (*f*) M. Prato, K. Kostarelos and A. Bianco, *Acc. Chem. Res.*, 2008, **41**, 60; (*g*) E. Miyako, H. Nagata, K. Hirano, Y. Makita, K.-i. Nakayama and T. Hirotsu, *Nanotechnology*, 2007, **18**, 475103; (*h*) M. J. O'Connell, S. M. Bachilo, C. B. Huffman, V. C. Moore, M. S. Strano, E. H. Haroz, K. L. Rialon, P. J. Boul, W. H. Noon and C. Kittrell, *Science*, 2002, **297**, 593.
2 P. C. Ma, B. Z. Tang and J.-K. Kim, *Carbon*, 2008, **46**, 1497.
3 M. J. Biercuk, M. C. Llaguno, M. Radosavljevic, J. K. Hyun and A. T. Johnson, *Appl. Phys. Lett.*, 2002, **80**, 2767.
4 S. A. Curran, P. M. Ajayan, W. J. Blau, D. L. Carroll, J. N. Coleman, A. B. Dalton, A. P. Davey, A. Drury, B. McCarthy, S. Maier and A. Strevens, *Adv. Mater.*, 1998, **10**, 1091.
5 Y. Saito and S. Uemera, *Carbon*, 2000, **38**, 169.
6 D. Qian, E. C. Dickey, R. Andrews and T. Rantell, *Appl. Phys. Lett.*, 2000, **76**, 2868.
7 (*a*) A. Hirsch and O. Vostrowsky, *Top. Curr. Chem.*, 2005, **245**, 193; (*b*) C. N. R. Rao, B. Satishkumar, A. Govindaraj and M. Nath, *ChemPhysChem*, 2001, **2**, 78; (*c*) S. Niyogi, M. A. Hamon, H. Hu, B. Zhao, P. Bhowmik, R. Sen, M. E. Itkis and R. C. Haddon, *Acc. Chem. Res.*, 2002, **35**, 1105; (*d*) M. Vaysse, M. K. Khan and P. Sundararajan, *Langmuir*, 2009, **25**, 7042; (*e*) T.-T.-T. Nguyen, F.-X. Simon, M. Schmutz and P. J. Mesini, *Chem. Commun.*, 2009, 3457.
8 (*a*) D. Tasis, N. Tagmatarchis, V. Georgakilas and M. Prato, *Chem.–Eur. J.*, 2003, **9**, 4000; (*b*) D. E. Hill, Y. Lin, A. M. Rao, L. F. Allard and Y. P. Sun, *Macromolecules*, 2002, **35**, 9466; (*c*) M. F. Islam, E. Rojas, D. M. Bergey, A. T. Johnson and A. G. Yodh, *Nano Lett.*, 2003, **3**, 269.
9 S. S. Karajanagi, H. Yang, P. Asuri, E. Sellitto, J. S. Dordick and R. S. Kane, *Langmuir*, 2006, **22**, 1392.
10 (*a*) B. Gigliotti, B. Sakizzie, D. S. Bethune, R. M. Shelby and J. N. Cha, *Nano Lett.*, 2006, **6**, 159; (*b*) M. Zheng, A. Jagota, E. D. Semke, B. A. Diner, R. S. McLean, S. R. Lustig, R. E. Richardson and N. G. Tassi, *Nat. Mater.*, 2003, **2**, 338.
11 (*a*) M. George and R. G. Weiss, *Acc. Chem. Res.*, 2006, **39**, 489; (*b*) R. G. Weiss and P. Terech ed., Springer: Netherlands, 2005, 613; (*c*) A. Srivastava, S. Ghorai, A. Bhattacharjya and S. Bhattacharya, *J. Org. Chem.*, 2005, **70**, 6574; (*d*) S. Bhattacharya and Y. K. Ghosh, *Chem. Commun.*, 2001, 185; (*e*) S. Bhattacharya, S. N. G. Acharya and A. R. Raju, *Chem. Commun.*, 1996, 2101; (*f*) A. R. Hirst, I. A. Coates, T. R. Boucheteau, J. F. Miravet, B. Escuder, V. Castelletto, I. W. Hamley and D. K. Smith, *J. Am. Chem. Soc.*, 2008, **130**, 9113; (*g*) A. Pal, Y. K. Ghosh and

S. Bhattacharya, *Tetrahedron*, 2007, **63**, 7334; (*h*) S. Bhattacharya and A. Pal, *J. Phys. Chem. B*, 2008, **112**, 4918; (*i*) K. G. Ragunathan and S. Bhattacharya, *Chem. Phys. Lipids*, 1995, **77**, 13; (*j*) S. Bhattacharya and S. N. G. Acharya, *Chem. Mater.*, 1999, **11**, 3121.

12 (*a*) T. Fukushima, A. Kosaka, Y. Ishimura, T. Yamamoto, T. Takigawa, N. Ishii and T. Aida, *Science*, 2003, **300**, 2072; (*b*) T. Fukushima, K. Asaka, A. Kosakaa and T. Aida, *Angew. Chem., Int. Ed.*, 2005, **44**, 2410.

13 (*a*) S. Bhattacharyya, S. Guillot, H. Dabboue, J.-F. Tranchant and J.-P. Salvetat, *Biomacromolecules*, 2008, **9**, 505; (*b*) M. Yoshida, N. Koumura, Y. Misawa, N. Tamaoki, H. Matsumoto, H. Kawanami, S. Kazaoui and N. Minami, *J. Am. Chem. Soc.*, 2007, **129**, 11039; (*c*) S. Srinivasan, S. S. Babu, V. K. Praveen and A. Ajayaghosh, *Angew. Chem., Int. Ed.*, 2008, **47**, 5746; (*d*) D. Shao, Z. Jiang, X. Wang, J. Li and Y. Meng, *J. Phys. Chem. B*, 2009, **113**, 860; (*e*) T. Fujigaya, T. Morimoto, Y. Niidome and N. Nakashima, *Adv. Mater.*, 2008, **20**, 3610; (*f*) E. Miyako, H. Nagata, K. Hirano and T. Hirotsu, *Adv. Mater.*, 2009, **21**, 2819; (*g*) Z. Hongbing, C. Wenzhe, W. Minquan, Zhengchan and Z. Chunlin, *Chem. Phys. Lett.*, 2003, **382**, 313; (*h*) Y. Wang, R. Cheng, L. Liang and Y. Wang, *Compos. Sci. Technol.*, 2005, **65**, 793; (*i*) F. Xiao, L. Liu, J. Li, J. Zeng and B. Zeng, *Electroanalysis*, 2008, **20**, 2047; (*j*) K. A. Dubey, Y. K. Bhardwaj, C. V. Chaudhari, V. Kumar, N. K. Goel and S. Sabharwal, *eXPRESS Polym. Lett.*, 2009, **3**, 492; (*k*) S. R. Sivakkumar and D.-W. Kim, *J. Electrochem. Soc.*, 2007, **154**, A134; (*l*) J. H. Rouse, *Langmuir*, 2005, **21**, 1055; (*m*) C. Liu, J. Zhang, J. He and G. Hu, *Polymer*, 2003, **44**, 7529; (*n*) H. G. Chae, M. L. Minus, A. Rasheed and S. Kumar, *Polymer*, 2007, **48**, 3781; (*o*) C. J. Ferris and M. in het Panhuis, *Soft Matter*, 2009, **5**, 1466.

14 (*a*) S. Bhattacharya, A. Srivastava and A. Pal, *Angew. Chem., Int. Ed.*, 2006, **45**, 2934; (*b*) A. Pal, A. Srivastava and S. Bhattacharya, *Chem.–Eur. J.*, 2009, **15**, 9169; (*c*) H. Basit, A. Pal, S. Sen and S. Bhattacharya, *Chem.–Eur. J.*, 2008, **14**, 6534.

15 A. Pal, B. S. Chhikara, A. Govindaraj, S. Bhattacharya and C. N. R. Rao, *J. Mater. Chem.*, 2008, **18**, 2593.

16 (*a*) S. K. Samanta, A. Pal and S. Bhattacharya, *Langmuir*, 2009, **25**, 8567; (*b*) S. Bhattacharya and S. K. Samanta, *Langmuir*, 2009, **25**, 8378; (*c*) S. K. Samanta, A. Gomathi, S. Bhattacharya and C. N. R. Rao, *Langmuir*, 2010, **26**, 12230.

17 (*a*) S. R. C. Vivekchand, A. Govindraj, M. M. Seikh and C. N. R. Rao, *J. Phys. Chem. B*, 2004, **108**, 6935; (*b*) S. R. C. Vivekchand, R. Jayakanth, A. Govindraj and C. N. R. Rao, *Small*, 2005, **1**, 920; (*c*) C. N. R. Rao and A. Govindaraj, *Nanotubes and Nanowires*, RSC Publishing, Cambridge, UK, 2005.

18 (*a*) S. J. George and A. Ajayaghosh, *Chem.–Eur. J.*, 2005, **11**, 3217; (*b*) P. Jonkheijm, F. J. M. Hoeben, R. Kleppinger, J. van Herrikhuyzen, A. P. H. J. Schenning and E. W. Meijer, *J. Am. Chem. Soc.*, 2003, **125**, 15941.

19 R. Sainz, A. M. Benito, M. T. Martinez, J. F. Galindo, J. Sotres, A. M. Baro, R. Corraze, O. Chauvet and W. K. Maser, *Adv. Mater.*, 2005, **17**, 278.

20 (*a*) E. S. Cho, S. W. Hong and W. H. Jo, *Macromol. Rapid Commun.*, 2008, **29**, 1798; (*b*) B. C. Satishkumar, L. O. Brown, Y. Gao, C.-C. Wang, H.-L. Wang and S. K. Doorn, *Nat. Nanotechnol.*, 2007, **2**, 560; (*c*) Y. Gao, M. Shi, R. Zhou, C. Xue, M. Wang and H. Chen, *Nanotechnology*, 2009, **20**, 135705.

21 M.-K. Seo, J.-R. Lee and S.-J. Park, *Mater. Sci. Eng., A*, 2005, **404**, 79.

22 (*a*) H. Li, L. Wang, B. Zhao, P. Shen and S. Tan, *J. Polym. Sci., Part A: Polym. Chem.*, 2009, **47**, 3296; (*b*) P.-K. Wei, Y.-F. Lin and W. Fann, *Phys. Rev. B: Condens. Matter Mater. Phys.*, 2001, **63**, 045417; (*c*) K. Akagi, O. S. Shibata, R. Toyoshima, I. Osaka and H. Shirakawa, *Synth. Met.*, 1999, **102**, 1287.

23 Y.-T. Shieh and G.-L. Liu, *J. Polym. Sci., Part B: Polym. Phys.*, 2007, **45**, 1870.

24 (*a*) J. K. Tan, T. Kitano and T. Hatakeyama, *J. Mater. Sci.*, 1990, **25**, 3380; (*b*) Z. Zhou, S. Wang, L. Lu, Y. Zhang and Y. Zhang, *J. Polym. Sci., Part B: Polym. Phys.*, 2007, **45**, 1616.

25 R. G. Larson. *The Structure and Rheology of Complex Fluids*, Oxford University Press, New York, NY, 1999.

26 (*a*) A. Jover, F. Meijide, E. R. Nunez and J. V. Tato, *Langmuir*, 2002, **18**, 987; (*b*) F. M. Menger and A. V. Peresypkin, *J. Am. Chem. Soc.*, 2003, **125**, 5340.

27 Y. Yao, C. Liu and S. Fan, *Nanotechnology*, 2006, **17**, 4374.

28 C. Zhou, J. Kong and H. Dai, *Appl. Phys. Lett.*, 2000, **76**, 1597.

29 S. Banerjee, T. Hemraj-Benny and S. S. Wong, *Adv. Mater.*, 2005, **17**, 17.

30 (*a*) Y. Li and T. Tanaka, *Annu. Rev. Mater. Sci.*, 1992, **22**, 243; (*b*) Y. Qiu and K. Park, *Adv. Drug Delivery Rev.*, 2001, **53**, 321; (*c*) C. C. Lin and A. T. Metters, *Adv. Drug Delivery Rev.*, 2006, **58**, 1379.

31 N. W. S. Kam, M. O'Connell, J. A. Wisdom and H. Dai, *Proc. Natl. Acad. Sci. U. S. A.*, 2005, **102**, 11600.

32 H. Tsuju, M. Moriyama, D. Nakayama, R. Ishii and R. Akashi, *Macromolecules*, 2006, **39**, 2291.

